Pages: 131-144 / Vol. 18 / Issue 1 / Winter-Spring 2025

Journal of Aerospace Science and Technology

Journal Homepage: https://jast.ias.ir

Original Research Article

Computational Modeling of Air-based Missiles Separation from Fighter Airplanes Using Six-degree-of-freedom Simulation with the Presence of the Thrust Force

Hossein Ansarian[1]* and Mostafa Hadidoolaabi [2]

1. Department of Aerospace Research Institute, Malek Ashtar University of Technology, Tehran, Iran

TICLE INFO

Received: 30 May 2024
Revised: 20 June 2024
Accepted: 23 June 2024
Available online: 01 April 2025

KEYWORDS:

Store separation
Six-degree-of-freedom simulation
Plume
Launcher
CFD

ABSTRACT

Numerical simulations have been performed to study the separation process of two air-launched missiles (Phoenix and AIM9X) from fighter airplanes (F-14 and F-5). Two launching mechanisms, rail launch and ejector launch, were modeled. Two aspects of safe separation were investigated, i.e. the missile should not collide physically with the airplane parts, and the rocket plume should not invade the airplane skin and not affect the engine inlet. The computational framework consists of a transient density-based flow solver, a dynamic unstructured mesh, a six-degree-of-freedom rigid body dynamics suite, and thrust force modeling. The thrust force has been modeled in two ways. The first method applies a dynamic force vector acting on the missile without the presence of the plume. The second method applies a pressure inlet boundary condition to simulate the exhausting plume. The technique has been verified with experimental data, and the results are presented by demonstrating the missile motion and trajectory parameters plots.

DOI: https://doi.org/10.22034/JAST.2024.460263.1189

1 INTRODUCTION

Store separation research involves predicting the flight characteristics of a projectile in the close vicinity of aircraft and other stores. Missiles launched from aircraft pass through complex flow fields. Regions with large velocity gradient exist because shock waves are emitted from the aircraft's nose, wings, leading edges, and canards. Also, due to side wash from the swept-back wings and downwash from the deflected canards, the missile experiences severe flow angularities. Although the non-uniform flow region is limited to near the aircraft, its influence is quite important. The complexity of the flow field causes the store to exhibit certain behaviors that may compromise the aircraft's safety or the missile's effectiveness. The store separation path should be safe and not show any dangerous motion toward the aircraft. The transitory effects of the separation process should not endanger the store's ability to complete the intended mission. The lateral motion can be the main

* Corresponding Author's Email: hossein.ansarian@gmail.com

Print ISSN:1735-2134 Online ISSN: 2345-3648

concern in some cases because of the small distances between the store and the adjacent aircraft parts or other stores [1, 2]. The trajectory is considered safe if the store leaves the aircraft flow field with increasing separation distance. In addition to the geometrical interference, the thermal interference of the hot exhausting plume of the missile rocket motor with the aircraft's body is regarded as a major concern. Because the missile is fired from a very close vicinity of the aircraft, especially for missiles with a rail-launch mechanism, the hot jet exhausting from the air-launched missiles can damage the sensitive parts of the aircraft's skin and adversely affect the intake systems, which may cause engine blowout and failure.

Generally, store separation research is performed with the aid of flight tests [3], experimental methods [4, 5], and computational methods [6]. Online or integrated methods [7] and offline or grid methods [8, 9] are typically applied in store separation dynamics. The first approach integrates a rigid body dynamics (RBD) solver with a CFD solver. The aerodynamic forces on the missile are computed using the numerical solver and then integrated by the RBD solver to obtain the current position of the store relative to the aircraft. This cycle is iterated until the missile gets away to a safe distance. The primary challenge in store separation dynamics prediction using numerical methods is the mesh generation over the complex geometries of flying vehicles. Structured grid solvers [9], dynamic unstructured grid solvers [11], overset mesh methods [12], and meshless methods [13] have been successfully used to simulate the store separation dynamics. In addition to the flow field nonlinearity, the uncertainties due to changes in missile mass properties, wing, fin, and thrust misalignments also contribute to the missile's undesirable flight characteristics or unsafe separation. Osman et al. [14] performed a store separation simulation for a generic store separating from an F-16 fighter using an unstructured dynamic grid. They reported that the results of the quasi-steady approach agree well with the experimental data. Berglind and Tysell [15] performed the store separation investigations with the aircraft maneuver. They reported that the separation process is safer during maneuver because of the simultaneous motion of the aircraft away from the projectile and the fact that the trajectory is weakly affected. Perillo and Atkins [16] pointed out that the significance of store separation research is growing because the stores' weight and size are rapidly diminishing, while their complexity and agility are increasing. Kapulu and Tekinalp [17] gave simulation results to predict the behavior of a store launched from a helicopter. They presented the effect of different inflow models on the collision of the helicopter body with the store. The simulation solver could predict unsafe cases and be employed as an effective analytical tool for determining critical flight situations before real flight tests. Recently, hybrid RANS/LES models have been used to simulate the store separation process from weapons compartments [18]. Anandhanarayanan et al. [19, 20] used an integrated store separation dynamics (SSD) code that consists of a meshless Euler solver, an RBD code, and a pre-processor, to simulate the dynamics of an agile air-to-air missile separation from a fighter aircraft at different flight conditions. The SSD tool can predict the flow field influence on the unguided missile trajectory, which is launched from the flying fighter aircraft.

The simulation of its path can investigate the plume impingement and its destructive effects during separation. The plume trajectory can be captured as a feature along with the missile path using CFD. Such a simulation might need solving the unsteady Navier-Stokes equations coupled with chemical equations or equivalent properties of gas, which requires massive computing resources. Usually, the isolated rocket plume shape is attached at the base as an extended part of the missile along its trajectory, computed using CFD. The modeled plume moves like a flashlight connected to the base and this approach is called the flashlight plume method [21]. However, treating the plume as a rigid body attached to the missile base is not realistic. It does not give true information about the actual thermal interference caused by the plume impingement. The particle integration method [22, 23] defines a cloud of particles injected continuously from the nozzle exit to the flow field as the missile gets away from the plane. The particles are followed in the direction of their velocity vector. The plume properties, such as species and local temperature, are interpolated from the isolated plume flow solution as functions of lateral and longitudinal displacement. Anandhanarayanan et al. [24] used this

method integrated with their meshless Euler solver-based SSD tool to compute the plume path for an air-to-air missile launched from a fighter plane.

In the present work, CFD is employed to predict the path of a missile just after being launched from a fighter airplane. Two air-to-air missiles, Phoenix and AIM9-X, are selected with two launch mechanisms, rail and ejectors. Numerical simulation for the rail-launched mechanism has been performed with and without modeling the rocket plume. The trajectory parameters and instantaneous plume shape are demonstrated to study the safety of the launching process.

2 COMPUTATIONAL METHOD

Three distinct components construct the computational framework: flow solver, six-degree-of-freedom (6DOF) rigid body trajectory, and moving grid algorithm. The governing fluid-dynamic equations are solved computationally by the flow solver at each time step. The aerodynamic forces and moments acting on the store are obtained from this solution. By applying aerodynamic and body forces, the movement of the store is computed by numerical integration of the Newton-Euler equations of motion. Finally, the unstructured grid is updated to account for the geometry displacement within the domain. The commercial software ANSYS FLUENT 19.1 [25] provides all three components and is used for the above procedure. The 6DOF element in this procedure is implemented as a user-defined function (UDF). It is a C code written by the user, which is dynamically linked with the FLUENT solver at run time.

The dynamic grid algorithm applies two methods for modifying the mesh in each time step. If the displacement of the moving geometry is small, a localized smoothing method is employed i.e., nodes are displaced to improve cell quality, but their connectivity does not change. The new nodal locations are computed using a so-called spring-based smoothing method, where the edges of the cell are considered as a set of interconnected springs between nodes. The displacement of a boundary node is propagated into the volume grid due to the spring force produced by the contraction or elongation of the corresponding edges. When the displacement of the store is large compared to the local cell size, the smoothing method is no longer sufficient to keep cell quality. Thus, based on skewness and/or volume criteria, poor-quality cells are remeshed locally and agglomerated when necessary.

3 SOLUTION VERIFICATION

For verification, the computational approach is implemented on a generic wing/pylon/store geometry (Fig. 1). The Arnold Engineering Development Center [26] published benchmark experimental data for this geometry, which were used for several store separation computational studies [11-13, 15, 29, 30]. Available experimental results include surface pressure distributions and trajectory information at multiple instants in time. The origin of the coordinate system is placed at the center of gravity of the store while in storage. The main wing has a NACA 64A010 airfoil section, and the store fins have an NACA 0008 airfoil. Three grids, summarized in Table 1 and shown in Fig. 2, were generated for this study using Gambit 2.4.6 software. Grid cells are tetrahedral and were refined by refining the Delaunay triangular surface meshes. Adiabatic wall boundary conditions are set on the all wall surfaces. Pressure far-field condition is set at the lateral and upstream domain extents, located 100D from the global axis origin. A symmetry condition is used for the plane containing the wing root. The downstream boundary is located at 85D from the origin and was assigned the pressure outlet condition.

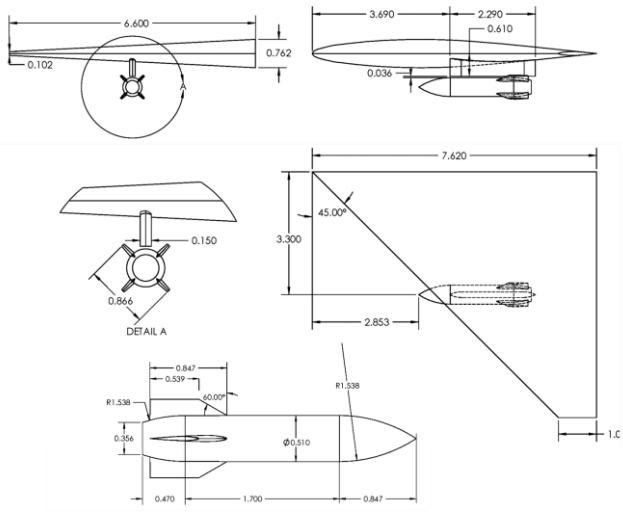

Fig. 1. Generic wing-pylon-store geometry (dimensions in m).

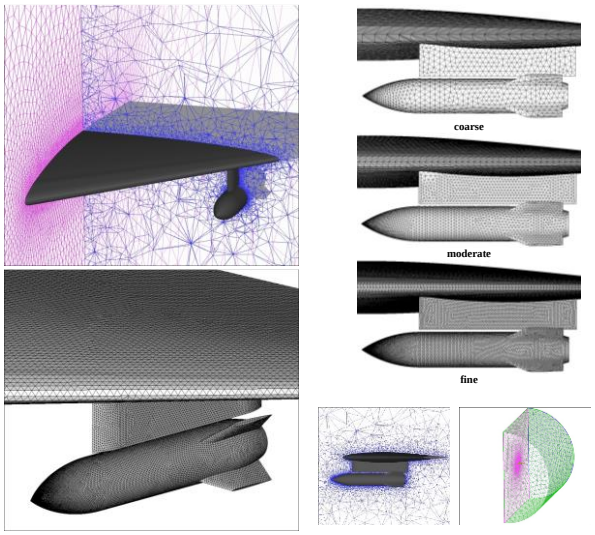

Fig. 2. Numerical grids around the generic geometry.

Table 1. Grid levels for the generic geometry.

Grid	Surface cells in the store	Volume cells
Coarse	3946	54836
Moderate	10524	162134
Fine	38994	584195

The Simulation of the separation process has been performed for free stream M∞ = 1.2 and the altitude of 11600 m and a zero angle of attack. To ensure a safe launch, two ejectors are employed to accelerate the store away from the pylon (Fig. 3). A substantial nose-down pitching moment acts on the store while in the carriage. Therefore, the force exerted by the forward ejector is smaller than that of the aft ejector to counter this moment. These forces are modeled in the UDF file as a resultant force and a moment at the store's center of gravity location. Table 2 gives the full-scale store and ejector properties used by the 6DOF routine. The converged steady-state solution was used as the initial condition for the unsteady simulation.

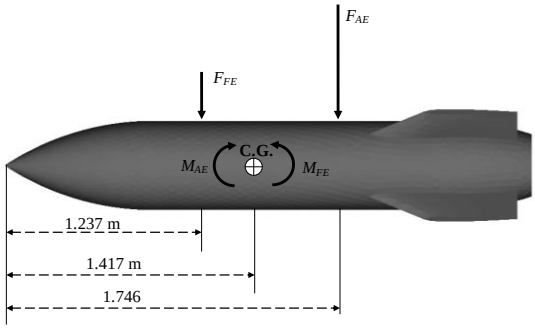

Fig. 3. Ejectors forces model.

Table 2. Store and ejectors properties.

Quantity	Value
Mass	907.kg
Center of gravity	1.42 m aft of nose
I_{xx}	27.12 kg.m^2
I_{yy}, I_{zz}	488.1 kg.m^2
Forward ejector location	1.24 m aft of nose
Aft ejector location	1.75 m aft of nose
Forward ejector force	10675 N
Aft ejector force	42702 N

An implicit transient density-based solver is used with an upstream 2nd-order AUSM scheme for the discretization of inviscid fluxes. Three time step values were tested to ensure Three time step values were tested to ensure the convergence of the trajectory: Δt = 0.01 s, Δt = 0.002 s, and Δt = 0.0004 s. At least 200 sub-iterations were run to ensure convergence in each time step. The computations were distributed over eight parallel processors to increase the speed. The separation process was simulated for 0.8 s. Fig. 4 shows the store movement with 0.2 s time intervals. Four trajectory parameters are extracted and compared with the experimental data: the location of the store center of gravity (CG), CG velocity, orientation (Euler angles), and angular rates. These parameters are plotted in Fig. 5-7. Each figure shows the CFD data and the experimental data for the three levels of mesh refinement.

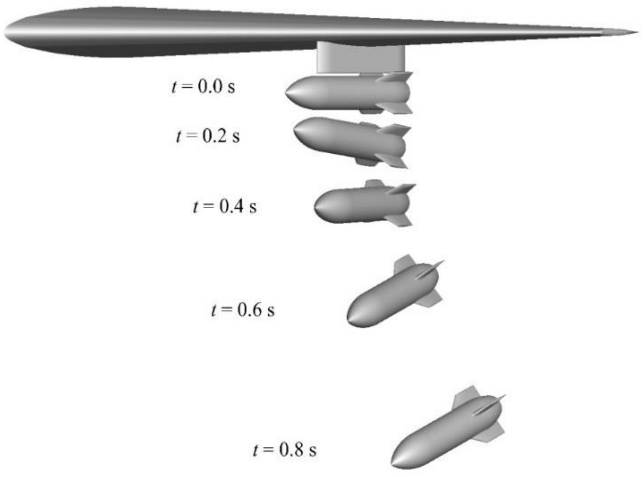

Fig. 4. Store location at different time steps.

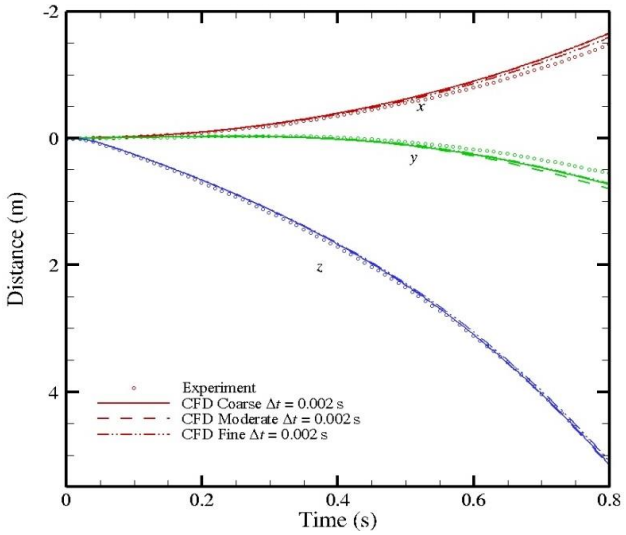

Fig. 5. CG locations for different grid levels.

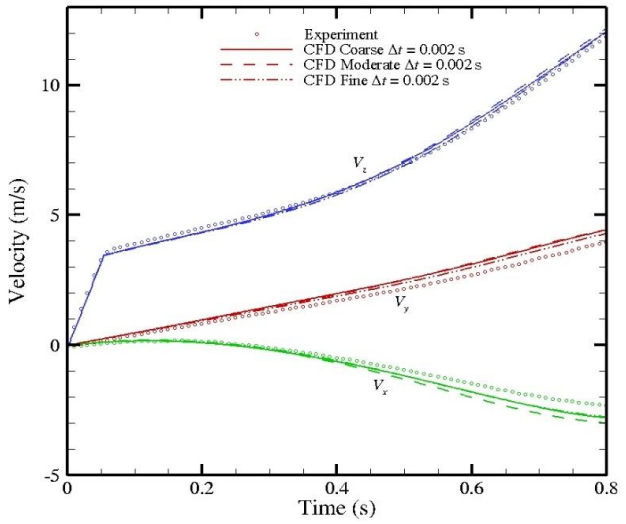

Fig. 6. CG velocity for different grid levels.

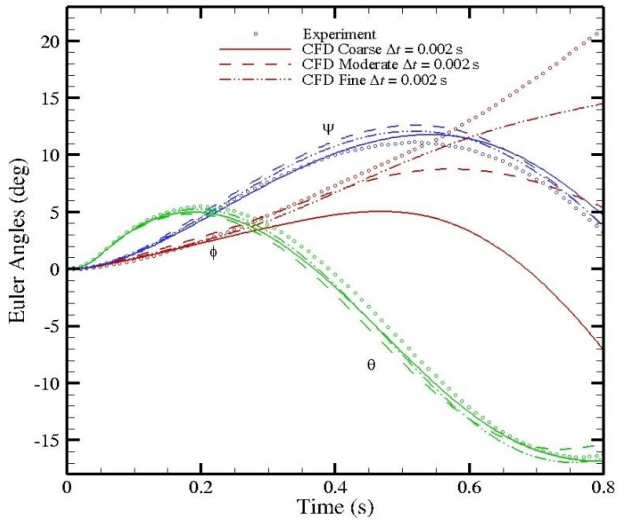

Fig. 7. Euler angles for different grid levels.

The store CG location in the global coordinate system is shown in Fig. 5 as a function of time. It is obvious that for all three grid refinements, the vertical location (z) agrees very well with the experimental data. This is because the ejectors and gravity forces are dominant compared to the aerodynamic forces in this direction. Also, in the x and y directions, a good matching is seen. The difference in the x direction is expected in the absence of viscous effects, but it becomes better by refining the grid. As the store falls, it moves rearward and slightly inboard. This is also seen in the CG velocities (Fig. 6). The store has a continuous rearward acceleration and is initially pulled slightly inboard, but it soon starts to move slowly outboard because of the wing outwash. As in the CG position, the velocity in the z direction agrees very well with the experiment. The effect of the ejection forces is clear at the start of the path as a large z-velocity gradient. At t = 0.05 s, the store is clear of the ejectors.

The variations of the Euler angles with time are shown in Fig. 7. The pitch and yaw angles match well with the experimental data. The moment produced by the ejectors makes the store to experience a nose-up pitch initially. After being released by the ejectors, the nose-down aerodynamic pitching moment reverses the trend. The store yaws initially outboard until approximately 0.55 seconds and then begins turning inboard. Throughout the first 0.8 seconds of the separation, the store rolls continuously outboard. CFD underpredicts this trend, and the curve tends to diverge from the experimental data after approximately 0.5 seconds. The roll angle is more difficult to capture since the moment of inertia about the longitudinal axis is too small compared to that of the two other axes. As a result, the roll motion is very sensitive to errors in the predicted aerodynamic forces. However, this estimation becomes better by refining the grid. The body angular rates are shown in Fig. 8. Again, it can be seen that the pitch and yaw rates match very closely with the experimental data, while the roll rate is more difficult to model.

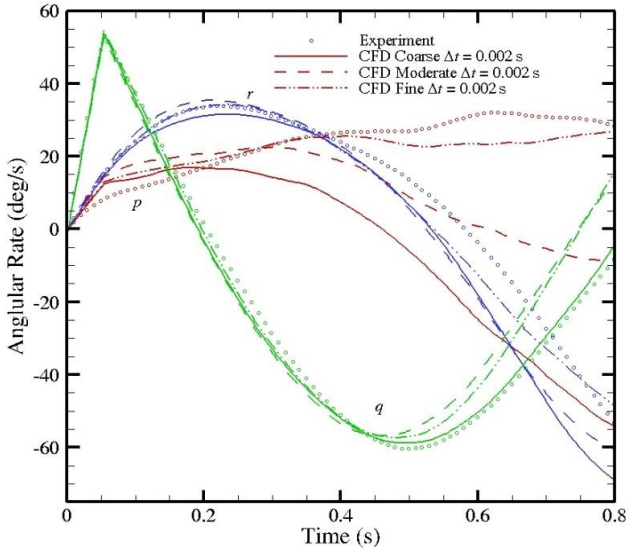

Fig. 8. Angular rates for different grid levels.

The time step effect on the above parameters is shown in Figures 9-12. The impact of the time step refinement is negligible on the CG position, except for the z direction. In terms of the orientation, $\Delta t = 0.0004$ s time step produces results with better agreement with the experimental results. The large time step size $\Delta t = 0.01$ s has been unsuccessful in predicting the Euler angles and their rates, and the results diverged from the experiment. In general, CFD had a good performance in simulating the store separation phenomenon. Refining the grid and time step size had more effect on the better prediction of Euler angles and rates compared to the CG location and linear velocities.

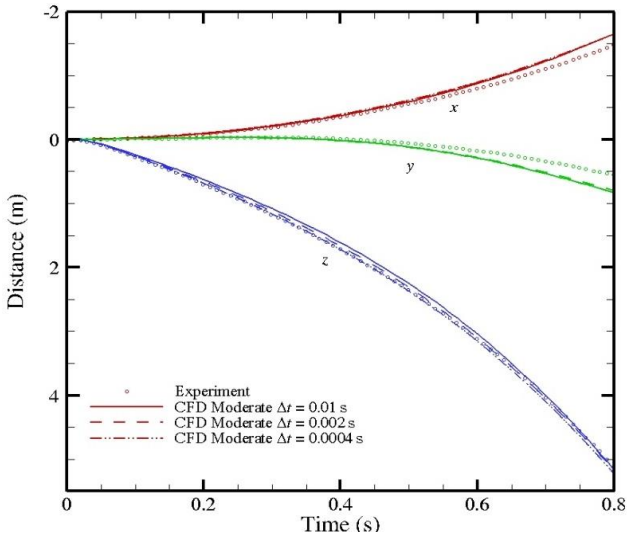

Fig. 9. CG locations for different time step sizes.

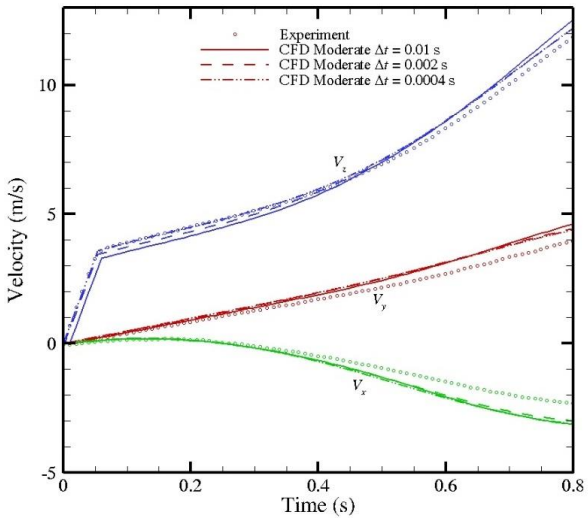

Fig. 10. CG velocity for different time step sizes.

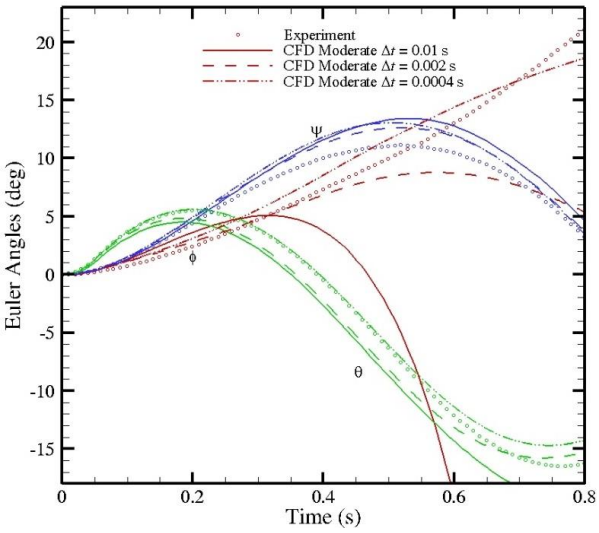

Fig. 11. Euler angles for different time step sizes.

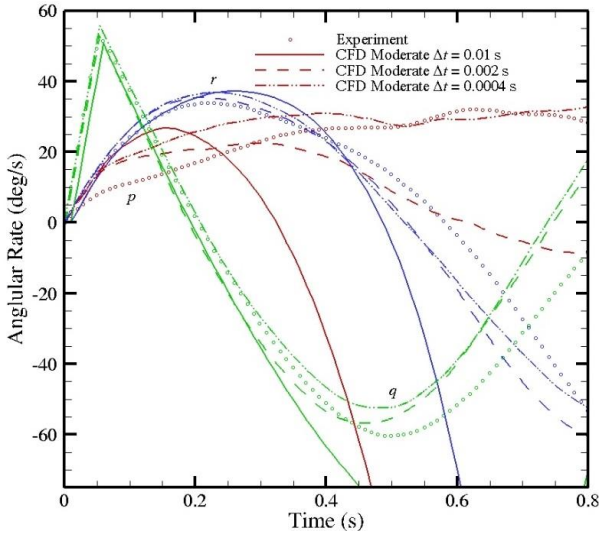

Fig. 12. Angular rates for different time step sizes.

4 SEPARATION OF THE PHOENIX MISSILE FROM THE F-14 FIGHTER

The numerical simulation of the separation of the Phoenix missile from the F-14 fighter has been performed and is presented in this section. The geometry and grids are shown in Fig. 13, which includes the full combination of fighter and missile and the launcher-pylon system. The computational method is similar to that used in the verification section, except that a viscous solution with k-ω SST turbulence model was used here. The boundary layer mesh was not generated because of the difficulties arising in the dynamic mesh; instead, a fine grid was generated on the missile surfaces. Table 3 shows the flight conditions and missile properties used in this simulation.

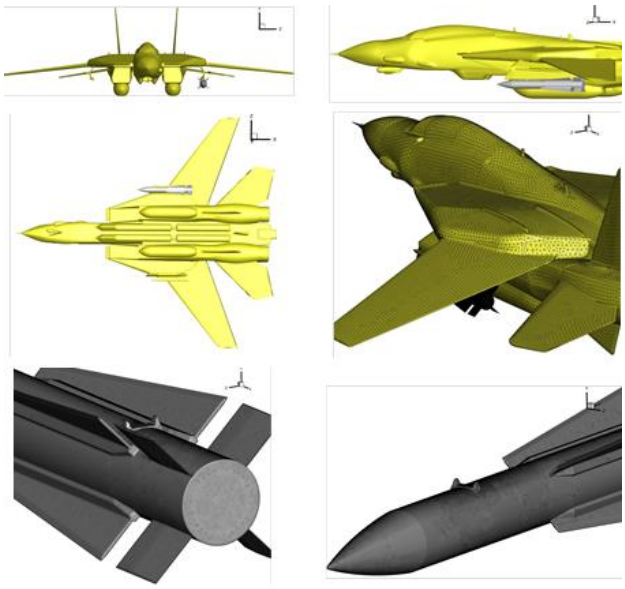

Fig. 13. Geometry and mesh for the F14-Phoenix Combination.

Table 3. Phoenix missile properties and flight conditions.

Quantity	Value
Mass	458 kg
Center of gravity	2.42 m aft of nose
I_{xx}	10.3 kg.m^2
I_{yy}, I_{zz}	349 kg.m^2
Forward ejector location	1.42 m aft of nose
Aft ejector location	3.26 m aft of nose
Forward ejector force	10675 N
Aft ejector force	42702 N
Maximum ejector force	104978 N
Ejector force duration time	0.1 s
Simulation time	0.27 s
Height	10 km
Mach number	0.5, 0.9, 1.1, 1.5
AoA	0

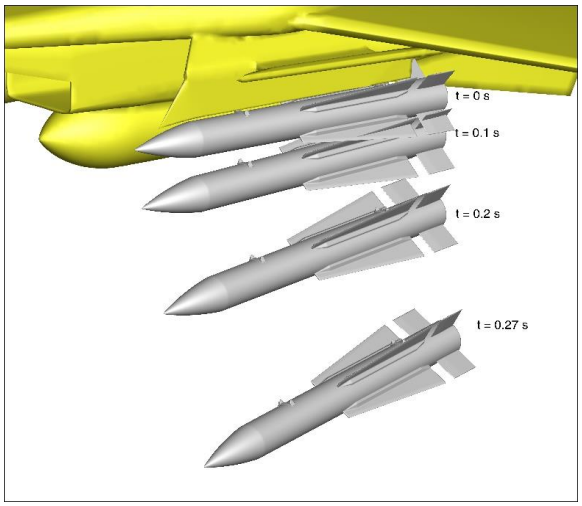

Fig. 14. Phoenix missile attitude at different time steps.

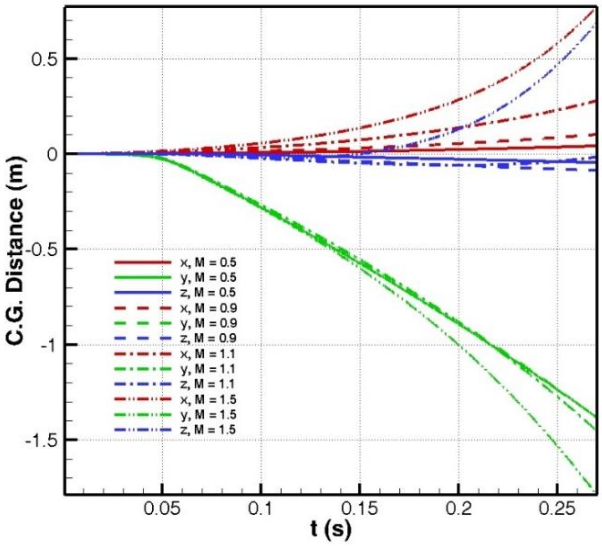

Fig. 15. Comparison of Phoenix CG location for different Mach numbers.

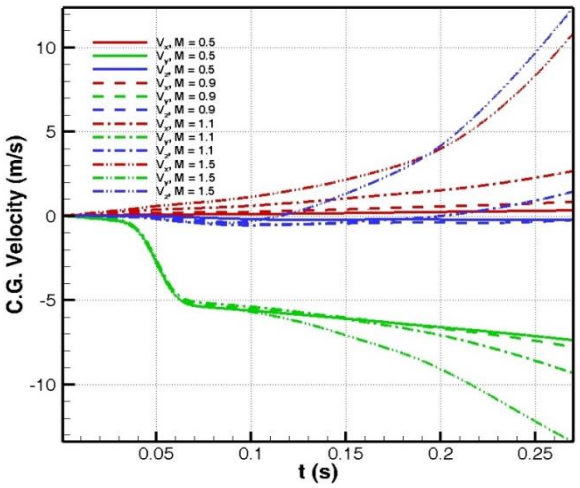

Fig. 16. Comparison of Phoenix CG velocity for different Mach numbers.

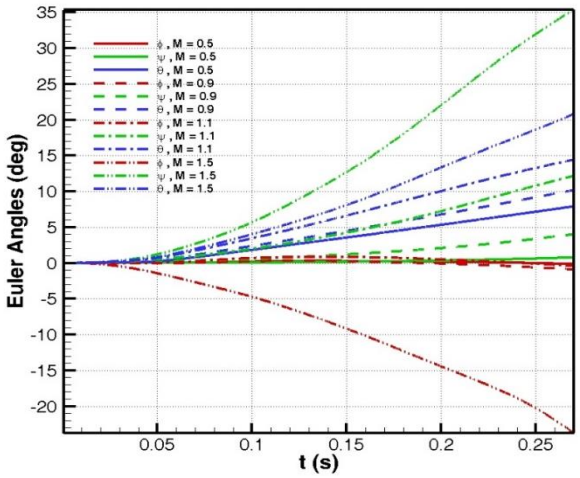

Fig. 17. Comparison of Phoenix Euler angles for different Mach numbers.

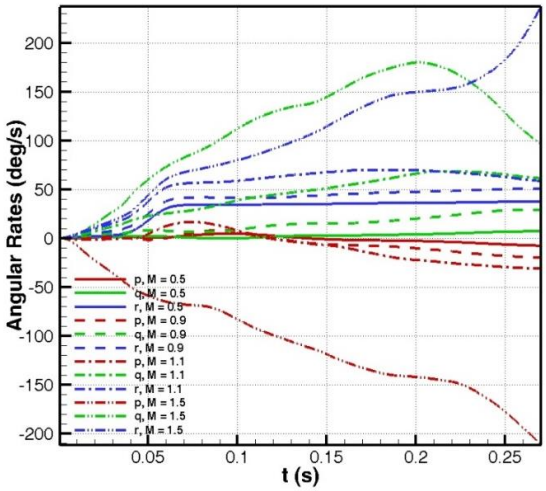

Fig. 18. Comparison of Phoenix angular rates for different Mach numbers.

5 SEPARATION OF THE AIM9-X MISSILE FROM THE F-14 FIGHTER

To simulate a separation process from a launcher with a rail mechanism, the AIM9-X Sidewinder missile was chosen and installed beneath the wing of an F-14 fighter. Fig. 19 shows the geometry and grids, and Table 4 shows the mass properties and flight conditions. Here, there is no ejector force, and the missile is launched through a sliding rail by its thrust force. A simple thrust-time profile is used and imposed as a vector force on the missile. It reaches from zero to 18 kN in 0.013 seconds and then remains constant. Using a transformation matrix, this vector is transformed to the missile body coordinates by receiving the Euler angles values at each time step. When the thrust force reaches 7 kN, the thrust locks are opened, and the missile is free for translational movement in the x direction, but its motion is restricted in the other directions until the second hook leaves the rail. Then it is allowed to take at most 1◦ pitch until the third hook leaves the rail, after which all motion constraints are removed.

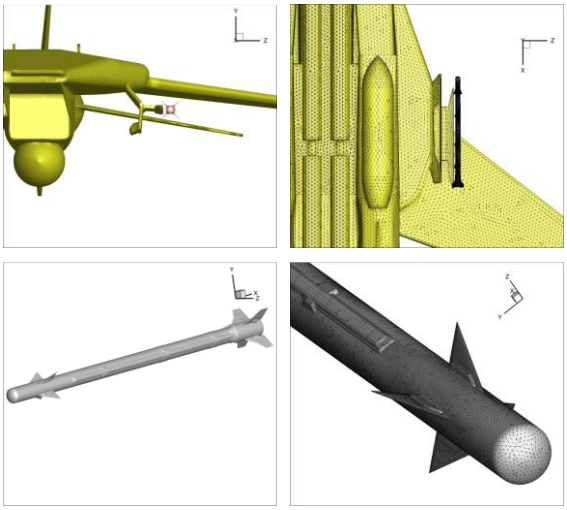

Fig. 19. Geometry and mesh for the F14-Sidewinder Combination.

Table 4. Phoenix missile properties and flight conditions**.**

Quantity	Value
Mass	81 kg
Center of gravity	1.6 m aft of nose
I_{xx}	0.26 kg.m^2
I_{yy}, I_{zz}	59.6 kg.m^2
Simulation time	0.6 s
Height	10 km
Free stream	M = 0.7˚, α = 3˚, 6˚, 9˚, -3˚ M = 0.85, α = 3˚

The numerical simulations have been performed for 0.6 seconds and five different flight conditions. Fig. 20 shows the missile motion for M = 0.7, α = 3° in 0.1-second snapshots. Fig. 21 shows the grid motion stages for the same case. Figs. 22-25 show the trajectory parameters for all simulated conditions. An approximately similar trend is observed for all conditions, and no dangerous proximity has occurred. The limitations exerted by the rail-launcher are obvious in the graphs.

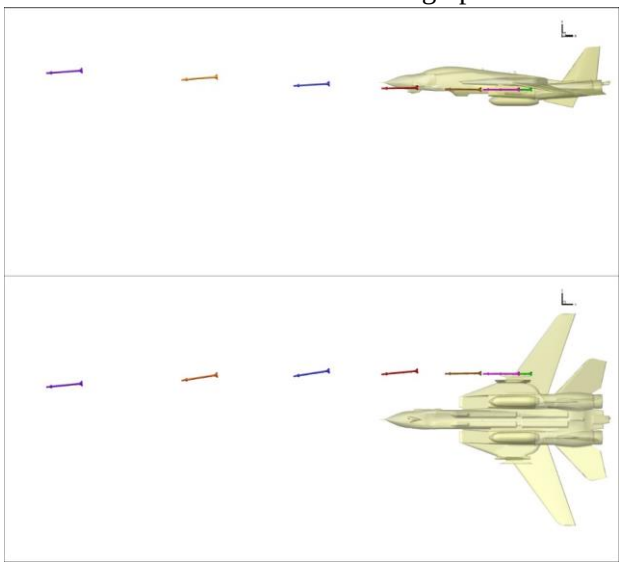

Fig. 20. AIM9-X location and attitude at different time steps

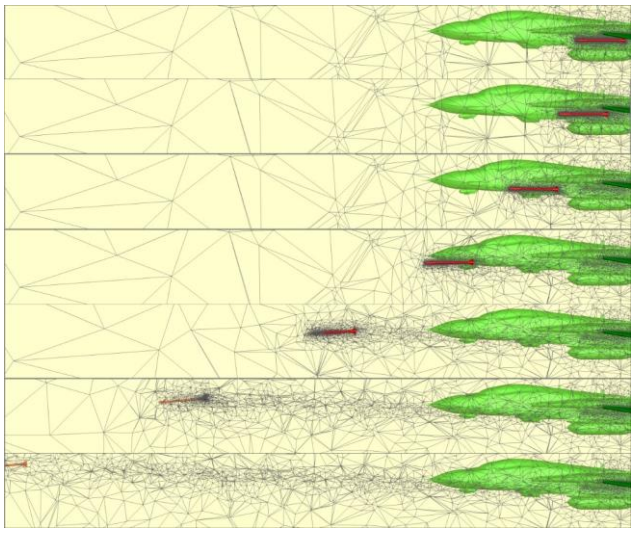

Fig. 21. Dynamic grid around AIM9-X – F-14 combination at different time steps

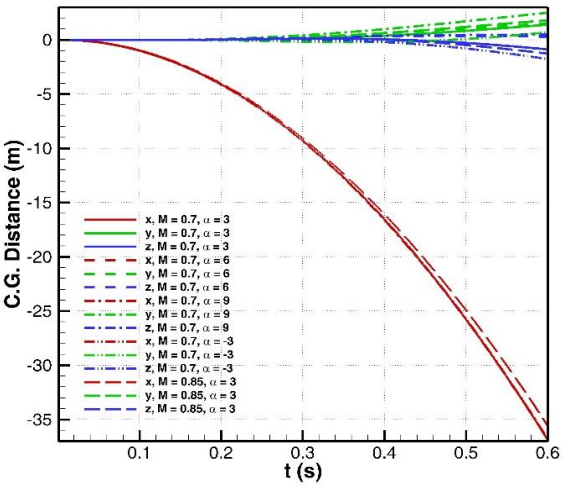

Fig. 22. Comparison of AIM9-X CG locations for different conditions.

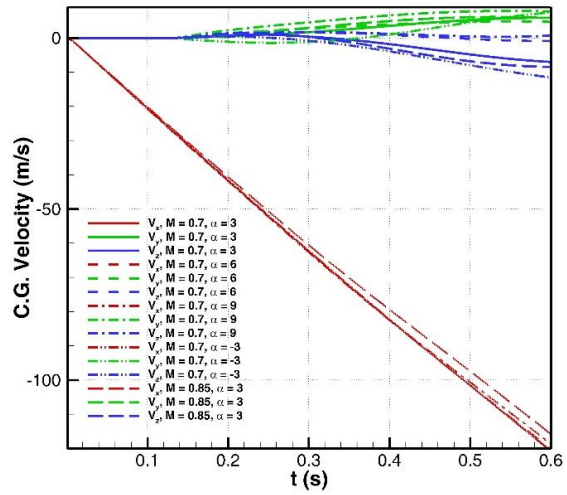

Fig. 23. Comparison of AIM9-X CG velocity for different conditions.

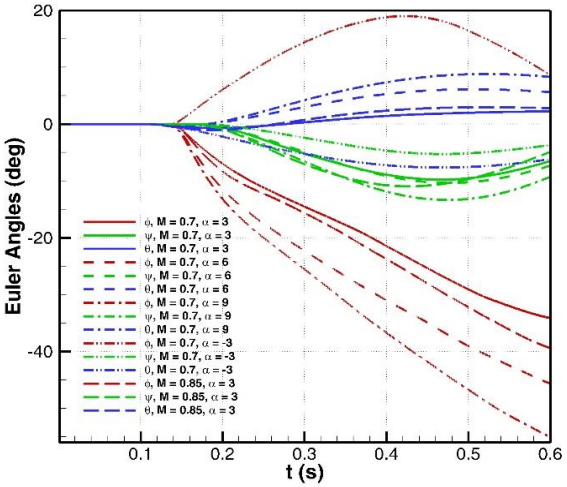

Fig. 24. Comparison of AIM9-X Euler angles for different conditions.

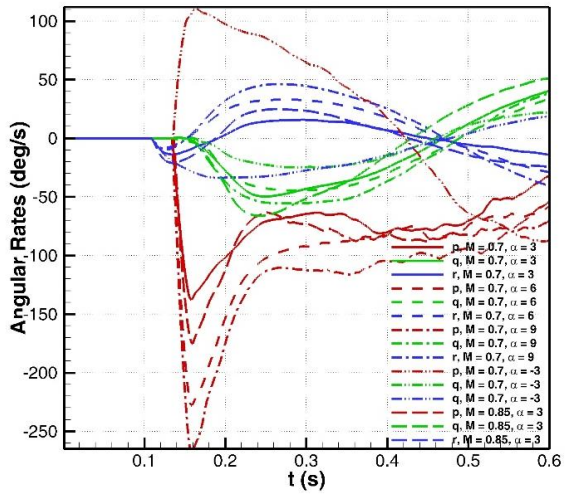

Fig. 25. Comparison of AIM9-X angular rates for different conditions.

6 SEPARATION OF THE AIM-9X MISSILE FROM THE F-5 FIGHTER WITH THE PRESENCE OF PLUME

To investigate the possible interference of the exhaust plume with airplane parts during the separation process, an AIM9-X missile installed on the wing tip rail launcher of an F-5 fighter is considered. The numerical simulation has been performed for h = 3 km, M = 0.7, α = 3°. The geometry and computational grid are shown in Fig. 26. The launcher mechanism is similar to the previous section. To model the jet plume, the missile geometry includes the combustion chamber and nozzle. However, instead of dealing with complex combustion equations, a pressure outlet boundary condition is imposed on the sidewall of the cylindrical chamber. A pressure profile, as shown in Fig. 27, is set for this boundary which provides the mass flow rate necessary for driving the missile. Air, as the working fluid, is defined as an ideal gas with a linear variation of constant pressure heat capacity (Cp). Cp value is 1006 j/(kg K) for free stream and 1920 j/(kg K) for T = 3050 K (equivalent to the combustion products). Since the pressure in the inlet boundary increases very rapidly, a smaller time step size was needed for this simulation; therefore, Δt = 10-5 was chosen, and the simulation was performed for 0.5 seconds.

Fig. 28 shows 0.1 s snapshots of the plume shape and size with the aid of a static temperature contour in the flow field. High temperature values are obvious in the combustion chamber, and the temperature levels close to the free stream value were eliminated. Fig. 29, shows a similar image from the front view but with the aid of a Mach number contour. From both figures, it can be seen that the plume zone has no physical interference with the airplane parts and is quite far from the engine inlet. Figure 30 shows the variations of static pressure on the airplane and missile surfaces. It is clear that there is no important change in the pressure value on the inlet walls, and the plume has not affected the inlet.

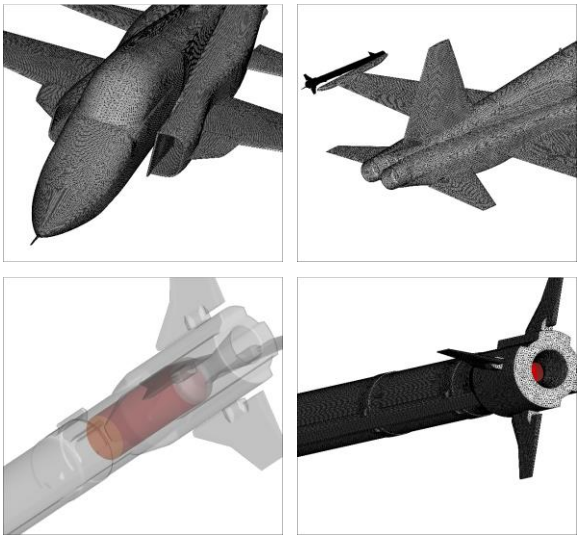

Fig. 26. Geometry and mesh for the F5-Sidewinder Combination

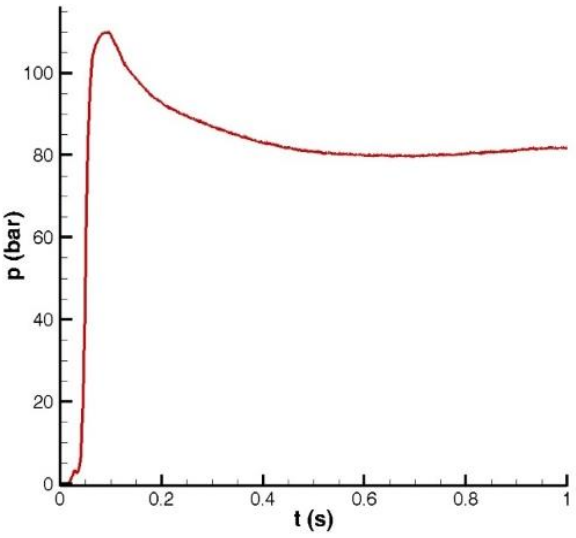

Fig. 27. Pressure time profile of the rocket motor

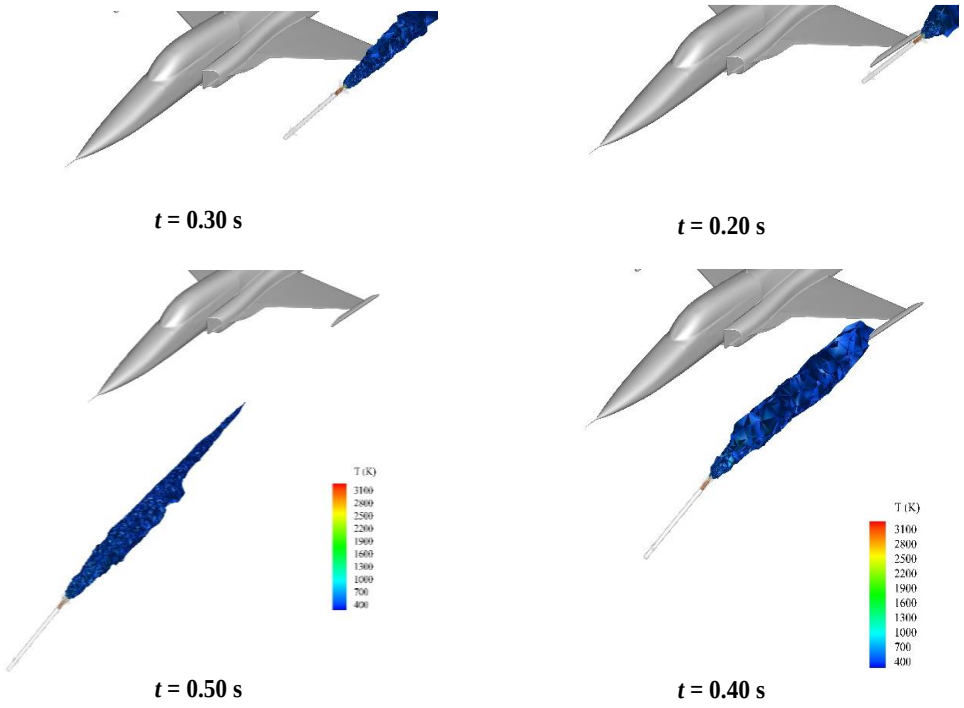

Fig. 28. Demonstration of plume using temperature contours at different time steps.

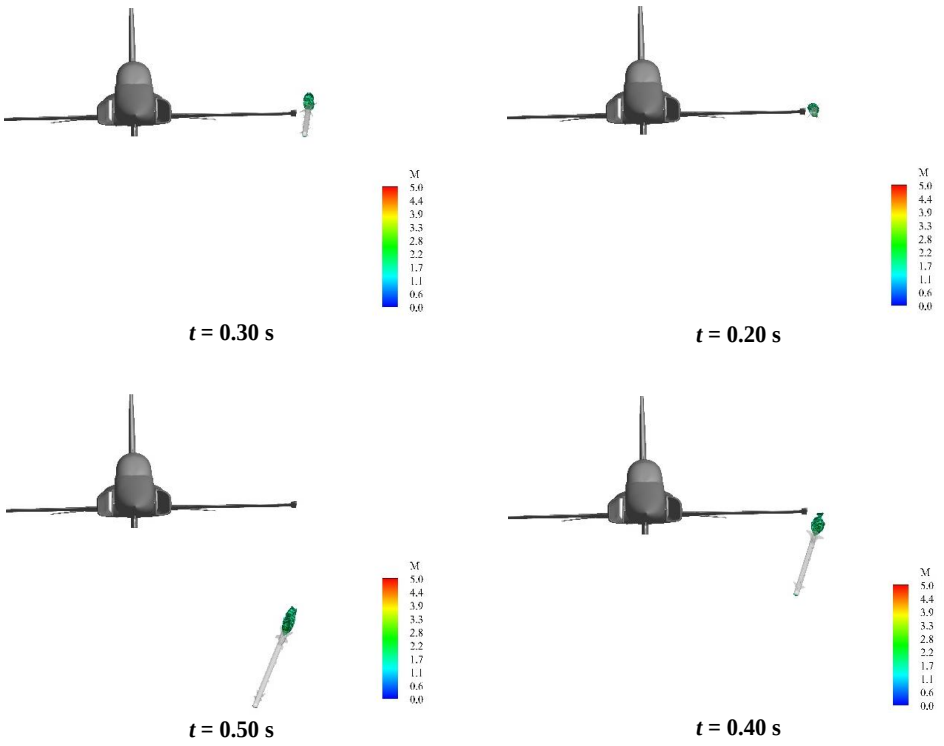

Fig. 29. Demonstration of plume using Mach number contours at different time steps.

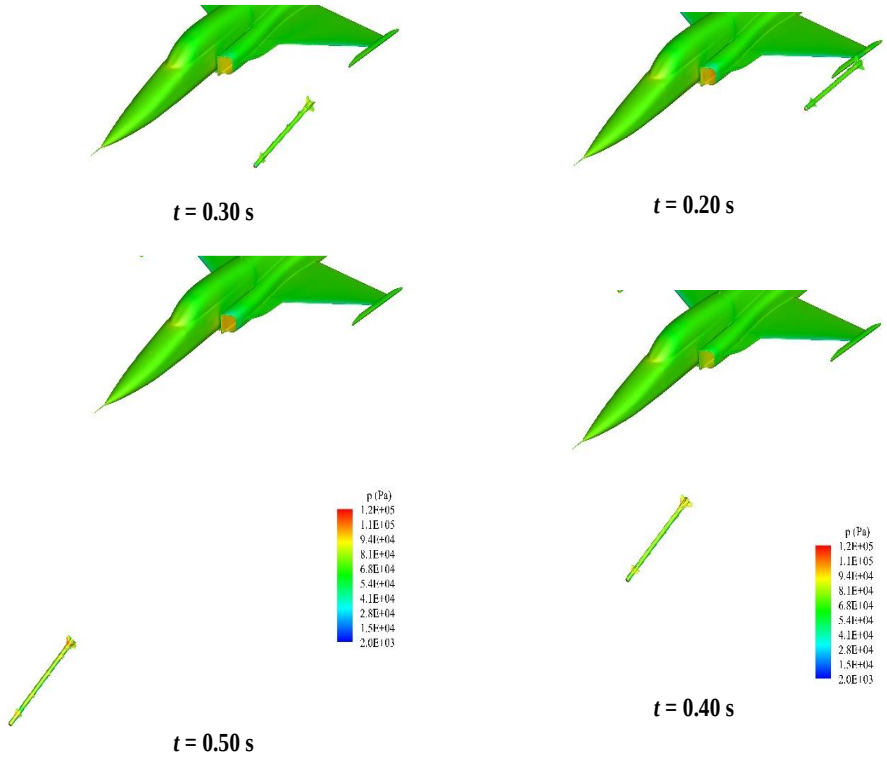

Fig. 30. Contours of static pressure over the F-5 and Sidewinder surfaces at different time steps.

7 CONCLUSION

Numerical simulations successfully investigated the separation process of air-launched missiles. Rail-launched and ejector-launched mechanisms were modeled for several flight conditions, and the effect of the rocket plume was investigated. The results showed safe separations for both selected missiles and all studied conditions, where no physical collision between missile and airplane parts was detected. Also, the jet plume had no interference with the airplane parts and did not affect the pressure distribution of the engine inlet. However, plots of trajectory parameters showed some severe motions, especially for Euler angles in the absence of a control system.

FUNDING

This research received no external funding.

CONFLICT OF INTEREST

The authors have nothing to disclose.

REFERENCES

[1] S. Chin, *Missile configuration design*, USA: McGraw-Hill Book Company, 1961.

[2] Fleeman EL. *Tactical missile design*. Virginia: AIAA, 2001.

[3] J. Hong Kim, C. Hyeon Sohn, I. Lee, and et al., "T-50/A-50 FSD Stores Separation Program." In: *AIAA Atmospheric Flight Mechanics Conference and Exhibit, Colorado*, USA, 21-24 August 2006, paper no. AIAA 2006-6000, https://doi.org/10.2514/6.2006-6000.

[4] Krekeler Jr G. C E.R., Popham, and D.R. Chaddock. F/A-II 8E/F weapons separation program. In: *37th Aerospace Sciences Meeting & Exhibit*, Reno, USA, ll-14 January 1999, paper no. AIAA 99-0394, https://doi.org/10.2514/6.1999-394.

[5] D.T. Veazey, "Current AEDC weapons separation testing and analysis to support flight testing." In: *USAF Developmental Test and Evaluation Summit, California*, USA, 16-18 November 2004, paper no. AIAA 2004-6847, https://doi.org/10.2514/6.2004-6847.

[6] W. Sickles, T. Hand, C. Morgret, J. Masters and A. Denny, "High-fidelity, time-accurate CFD store separation simulations from a B-1B bay with comparisons to quasi-steady engineering methods*." in: 46th AIAA Aerospace Sciences Meeting and Exhibit, Reno*, USA, 7 - 10 January 2008, paper no. AIAA 2008-186, https://doi.org/10.2514/6.2008-186.

[7] S. Lee, M. Park, K. Cho and J. Kwon, "A new automated chimera method for the prediction of store trajectory." in: *17th Applied Aerodynamics Conference, Norfolk*, USA, 28 June - 1 July 1999, paper no. AIAA-99-3131, https://doi.org/10.2514/6.1999-3131.

[8] M. Bamber, "Store separation investigations by grid method using wind tunnel data." *David Taylor Model Basin*, Rep. 2202, April 1966.

[9] S. Davids and A. Cenko, "Grid-based approach to store separation." in: *19th AIAA Applied Aerodynamics Conference*, Anaheim, USA, 11-14 June 2001, paper no. AIAA Paper 2001-2418, https://doi.org/10.2514/6.2001-2418.

[10] Scott M. Murman, Michael J. Aftosmis and Marsha J. Berger, "Simulations of store separation from an F/A-18 with a Cartesian Method." *J Aircr 2004;* vol. 41, pp.870-878, 2004, https://doi.org/10.2514/1.473.

[11] D. Snyder, E. Koutsavdis and J. Anttonen. "Transonic store separation using unstructured CFD with dynamic meshing." in: *33rd AIAA Fluid Dynamics Conference and Exhibit, Orlando*, USA, 23-26 June 2003, paper no. AIAA 2003-3919, https://doi.org/10.2514/6.2003-3919.

[12] L. E. Lijewski and N. E. Suhs. "Time-accurate computational fluid dynamics approach to transonic store separation trajectory prediction." *J Aircr*. vol. 31, 1994, pp. 886-891, https://doi.org/10.2514/3.46575.

[13] G. Harish, M. Pavanakumar and K. Anandhanarayanan, "Store separation dynamics using grid-free Euler solver." *in: AIAA 24th Applied Aerodynamics Conference*, San Francisco, USA, June 2006, paper no. AIAA paper 2006 3650, https://doi.org/10.2514/6.2006-3650.

[14] Alaa A. Osman, Amgad M. Aly, Essam E. Khalil, and Osama E. Abdelattif, "Numerical analysis of an external store separation from an airplane.: in: *AIAA Modeling and Simulation Technologies Conference*, San Diego, USA, 4-8 January 2016, paper no. AIAA 2016-2143, https://doi.org/10.2514/6.2016-2143.

[15] T. Berglind and L. Tysell, "Numerical investigation of the impact of maneuver on store separation trajectories." in: *28th AIAA Applied Aerodynamics Conference*, Chicago, USA, 28 June - 1 July 2010, paper no. AIAA 2010-4241, https://doi.org/10.2514/6.2010-4241.

[16] S. Perillo, D. Atkins, and W. Roberts, "Challenges and emerging trends in store separation engineering: an air force SEEK EAGLE Office perspective." in: *47th AIAA Aerospace Sciences Meeting Including The New Horizons Forum and Aerospace Exposition*, Orlando, USA, 5 - 8 January 2009, paper no. AIAA 2009-0101, https://doi.org/10.2514/6.2009-101.

[17] O. Kapulu and O. Tekinalp, "Main rotor downwash effect on separation characteristics of external stores." in: *AIAA Atmospheric Flight Mechanics Conference, Grapevine*, USA, 9 - 13 January 2017, paper no. AIAA 2017-1864, https://doi.org/10.2514/6.2017-1864.

[18] T. Rokita, R. Arieli and Y. Levy, "Different approaches for simulating the flow inside and near a weapons bay," in: *30th AIAA Applied Aerodynamics Conference, New Orleans*, USA, 25 - 28 June 2012, paper no. AIAA 2012-3339, https://doi.org/10.2514/6.2012-3339.

[19] K. Anandhanarayanan, "Development of three-dimensional grid-free solver and its applications to multi-body aerospace vehicles." *Def Sci J*., vol. 60, 2010, 653-662, https://doi.org/10.14429/dsj.60.583.

[20] K. Anandhanarayanan, A. Raj, V. Shah, and R. Krishnamurthy, "Separation dynamics of air-to-air missile and validation with flight data." *Def Sci J*., vol. 68, 2018, pp. 5-11, https://doi.org/10.14429/dsj.68.11480.

[21] R. Gleissl and R. Deslandes, "Simulation of missile plumes for aircraft store compatibility assessments." *in: 43rd AIAA Aerospace Science Meeting and Exhibit. Reno*, USA, 10 - 13 January 2005, paper no. AIAA 2005-54, https://doi.org/10.2514/6.2005-54.

[22] R. Gleissl, R. Deslandes, and A. Baeten, "Assessment of missile plume impact characteristics," in: *45th AIAA Aerospace Science Meeting and Exhibit*, Reno, USA, 8 - 11 January 2007, paper no. AIAA 2007-675, https://doi.org/10.2514/6.2007-675.

[23] R. Ankit and K. Anandhanarayanan, "Modeling of missile plume path during store separation." in:

Proceedings of Symposium on Applied Aerodynamics and design of Aerospace Vehicle (SAROD 2011), Bangalore, India, 16-18 November 2011,

[24] K. Anandhanarayanan, A. Raj, R. Krishnamurthy, and D. Chakraborty, Engineering method of prediction of plume path of air-launched missile. *Def Sci J.*, vol. 70, 2022, pp. 201-206, https://doi.org/10.14429/dsj.70.13853.

[25] Available, [online]: https://ansyshelp.ansys.com

[26] E. Ronalld Heim, "CFD wing/pylong/finned store mutual interference wind tunnel experiment." Rep. AEDC—TSR-91-P4, USA: Arnold Engineering Development Center, Air Force Systems Command, United States Air Force, 1991, 63pages.

[27] L.Tang, J. Yang, and J. Lee, "Hybrid Cartesian grid/gridless algorithm for store separation prediction." in: *48th AIAA Aerospace Sciences Meeting Including the New Horizons Forum and Aerospace Exposition*, Orlando, USA, 4 - 7 January 2010, paper no. AIAA 2010-508, https://doi.org/10.2514/6.2010-508.

[28] Y. Emre Sunay, E. Gülay, and A. Akgül, "Numerical simulations of store separation trajectories using the EGLIN test." *Scientific Technical Review*, vol. 63, no.1, 2013, pp.10-16, https://doi.org/10.2514/6.2018-1272.

[29] M. Sheharyar, E. Uddin, Z. Ali, Q. Zaheer, and A. Mubashar. "Simulation of a standard store separated from the generic wing." *J Appl Fluid Mech*; vol. 11, 2018, pp. 1579-1589, https://doi.org/10.29252/jafm.11.06.28865.

[30] S. Madasamy, B. Priyeswar, G. Thilagapathy, and et al., "Investigation of store separation and trajectory of weapons in military aircraft." *IJSER*, vol. 7, 2016, pp. 84-88.

COPYRIGHTS

Authors retain the copyright and full publishing rights.
Published by Iranian Aerospace Society. This article is an open access article licensed under the Creative Commons Attribution 4.0 International (CC BY 4.0).

HOW TO CITE THIS ARTICLE

H. Ansarian and M. Hadidoolaabi, "Computational Modeling of Air-based Missiles Separation from Fighter Airplanes Using Six-degree-of-freedom Simulation with the Presence of the Thrust Force," *Journal of Aerospace Science and Technology*, Vol. 18, Issue 1, 2025, pp. 131-144.

DOI: https://doi.org/10.22034/JAST.2024.460263.1189

URL: https://jast.ias.ir/article_198690.html